Tuijin Jishu/Journal of Propulsion Technology
ISSN: 1001-4055
Vol. 45 No. 3 (2024)

Computational Investigation of Stagnation Point Flow of Non-Newtonian Nanofluid on a Rotating Disk with Cattaneo-Christov Heat Flux

A. Bharathi[1], Mattipelli Ramachandru[2*], Ch. Kishore Kumar[3], S. Renuka[4], K. Sree Ram reddy[5], K. Satyanarayana[6]

[1]TGSWRDCW, Medak, Telangana, India- 502110
[2]UCE&T, Mahatma Gandhi University, Nalgonda, Telangana, India- 508254
[3, 4]Department of Mathematics, Nizam College, Osmania University, Telangana, India- 500001
[5,6]Department of Mathematics, UCS, Osmania University, Telangana, India- 500007

Abstract:- The exploration of fluid behavior on a rotating disk is crucial because it finds numerous uses across various sectors like engineering, science, and industry. Our present study focuses on examining how heat is transferred around a stagnation point in the flow of Casson nanofluid over a rotating disk. The investigation considers the flow of heat and the distribution of mass within the system, particularly regarding Cattaneo Christov heat flux and chemical reactions. Nonlinear partial differential equations are transformed into ordinary differential equations by the use of similarity transformations, resulting in a reduction in complexity. Subsequently, the Bvp4c method is employed to visualize the graphical outlines and our findings reveal that the fluid's ability to effectively conduct heat is influenced by several parameters. The velocity distribution decline with an increase viscoelastic parameter β, such as the Casson parameter values. Enhancing the Nb parameter improved the temperature distribution but, at the same time, negatively affected the Concentration profile. The outcomes of this research is beneficial in a variety of fields, including transportation, architectural engineering, enhancing oil extraction techniques, and medical applications involving nanofluids.

Keywords: Non-Newtonian Casson fluid, Rotating disk, Cattaneo Christov heat flux, Stagnation point, and Chemical reaction.

1. Introduction

The rotating disk model has garnered substantial interest as a means of examining various forced flow and heat transfer phenomena in non-Newtonian fluids. This is achieved via the use of analytical, computational, and experimental techniques to get a deeper understanding of their behavior. due to its inherent simplicity and ease of comprehension and replication. Both theoretically and practically, the rotation of disks may be beneficial. It has been used in purifying machineries, viscometers, physiological structure analysis, and material handling technology, medical equipment, oceanic research, and many other areas. Several contemporary technologies, such as those used in memory components, rely on the utilization of electrically charged fluids that spin in predetermined orientations. Instances of this kind of research include the advancement of nanocrystals and viscometers.

In 1921, Karman conducted an investigation on the fluid flow resulting from the rotation of a disk. The dynamic movement described by Navier's Stokes equations was converted into a set of ordinary equations by a recently introduced transformation. Karman provided these changes in this attempt, thus the term Karman transformation. Subsequently, several studies on rotational flows have been conducted utilizing the Von Karman technique. Turkyilmazoglu and Senel (2013) extended Karman's flow problem starting from 2013. The extended

investigation incorporates the heat transfer characteristics when fluid flow is achieved via a rotating disk under circumstances of partial

Nomenclature:-

(u,v,w)	-Velocity components	Nt	-Thermophorosis parameter
(r,φ,z)	-Cylindrical coordinates	Nb	-Brownian motion parameter
M	-Magnetic parameter	c,d	-Stretching constants
Sc, Pr	-Schmidt, Prandtl number	Bi	-Biot number
D_B, D_T	-Brownian diffusion		
Kr	-Chemical reaction	**Greek symbols**	
ρ_f	-Density of fluid	ϑ_f	-Kinematic viscosity
B_o	-Magnetic field strength	μ	-Dynamic viscosity
T_∞	-Free stream temperature(K)	β	-Casson parameter
T_f	-Surface temperature(K)	τ	-heat capacity
λ_1	-Thermal relaxation	γ	-Thermal relaxation time
C_∞	-Free stream Concentration	**Subscripts**	
k	-Thermal conductivity	f	-fluid
Re_r	-Reynolds number	∞	-Free stream
u_e	-Ambient velocity		

slip. Rashidi et al.(2014) studied the influence of entropy on velocity slip flow resulting from a porous spinning disk. Additionally, they explore the effects of magnetic fields. Turkyilmazoglu (2014) enhanced the novelty of the rotational flow problem by including Nano sized particles into the flow regime. He conducts a comparative analysis using many nanoparticles in the fluid flow regime.

The investigation of magnetohydrodynamic (MHD) non-Newtonian fluid flow at a stagnation point across a spinning disk is a challenging but crucial area of study with many practical implications. Studies have investigated Khan et.al (2023) the impact of magnetohydrodynamic, porous media, mixed convection, and micro-rotational effects on the behavior of fluids. In addition, studies have analyzed “the influence of mixed convection, thermal radiation, chemical processes, and Casson parameters on the velocity and temperature profiles, skin-friction coefficients, and Nusselt numbers” in comparable situations, Moreover, research has examined the impact of micro polar, magnetic, mixed convection, and radiation factors on the profiles of fluid velocity, angular velocity, and temperature distribution when a vertical sheet is exposed to exponential stretching or shrinking by Sulochana et al.92023) and Bakar et al.(2023). Furthermore, an investigation was conducted on the behavior of a water-based hybrid nanofluid that consists of ferrous and graphene oxide nanoparticles flowing past a flat plate. The study examined Dawar et.al (2022) the impact of magnetic fields and thermal radiation on the velocity and thermal fields. The results showed that these effects are influenced by the volume fractions of the nanoparticles and variations in the power-law index. Finally, a study has been conducted on the evaluation of MHD non-aligned stagnation-point flow over a surface that Stretch with a convective boundary condition in the presence of a porous medium. The study focuses on the impact of magnetic and porosity parameters on the profiles of velocity, temperature, and nanoparticle volume fraction by Katnurkar and Mali (2022). Rehman et al. (2018) conducted a numerical investigation on the flow yield of a magnetohydrodynamic (MHD) Casson fluid with Navier's slip nanofluid utilizing a rigid spinning disk. An investigation of the heat transfer that occurred close to the Stagnation Point of a Maxwell nanofluid flow that was traveling over a porous rotating disk was carried out by Li et al. (2024). Scholars in recent decades have

shown significant interest in investigating the flow stagnation at the point where it impinges on a rotating disk. Hannah (1947) studied the flow of a revolving disk that resulted in a stationary point flow when it impinged on a wall along a normal-to-the-wall axisymmetric direction. Agrawal (1957) examined the characteristics of a spinning across the flow.

Rehman et al. (2022) examined the effects of temperature and concentration diffusion on magnetohydrodynamic Maxwell fluids. This study has likely enhanced our comprehension of the interaction between magnetic fields and thermal/concentration effects in Maxwell fluids. Nanofluids have been developed as a means to address technological obstacles in areas such as solar energy collection, heat exchangers, and engine cooling by Hayat et.at (2017). Nanofluids are created by adding particles that are smaller than 100 nm in size to base fluids like as oil, water, biofluids, and ethyl. Choi(1995) implemented this notion by incorporating minuscule nanoparticles into a foundational fluid to augment its heat conductivity. The yield stress of a Casson fluid exceeds the shear stress. Moreover, when the shear stress exceeds the yield stress, materials having Casson fluid properties may display solid-like characteristics. The Casson fluid model is very reliable for predicting the behavior of blood, liquids, melted chocolate, sauces, and other similar suspensions. Studies on Casson liquid have garnered substantial attention from researchers and scientists discussed such as Nadeem et al. (2012), Mukhopadhyay (2013), Mahanta and Shaw (2015), Waqas et al.(2021) and Bhixapathi and Babu (2024).

An investigation of the MHD Cattaneo-Christov heat flux on a revolving disk is essential for a range of industrial uses, including air conditioning, machinery power collection, and thermal systems. The use of the Cattaneo-Christov heat flux model in examining the movement of nanofluids across spinning disks has been shown by research to provide significant understanding into the mechanics of heat transfer. Researchers have used numerical methods to solve the governing equations and observe “the effects of elements such as magnetic fields, nanoparticle concentrations, and thermal relaxation parameters on velocity, temperature, and heat transfer rates”. Furthermore, the examination of the flow of non-Newtonian nanofluid caused by a spinning disc that may stretch has emphasized the importance of Stefan blowing and its contribution to improving heat transmission and the concentration of nanoparticles. This finding might have ramifications in the field of medical treatments Noreen et al.(2023), Samantaray et al. (2023), Zeb et al.(2023), Moatimid et al. (2022) and Habu et al.(2022).

The area of heat transfer dynamics is widely used in both industry and biology. Fourier's law, derived from continuum mechanics, is often used to characterize heat conduction. Nevertheless, this rule has a notable limitation since it does not account for the time delay in heat transfer, making the model very impractical. In order to overcome this constraint, researchers further extended the law by including the time-lag component, leading to the development of the Cattaneo-Christov (CC model) heat flow model. Presently, there is a significant amount of attention focused on investigating the CC model. Several researchers Ali et al.(2022) and Ahmed et al.(2019) have analyzed the flow dynamics of nanofluid between coaxial disks using this model major uses of the Cattaneo-Christov model is its use in nanofluid modeling.

The present work included doing numerical calculations for the stagnation point flow model of a non-Newtonian nanofluid on a spinning disk that is heated by convection. This model incorporates chemical reactions, latent heat of fusion, and the Cattaneo-Christov heat flow. The importance of this research is in its diverse range of practical uses, namely in the domain of medical non-Newtonian fluids subjected to nanoparticles on a vertically rotating disc. The phenomena are formally represented as a system of partial differential equations (PDE). In order to streamline the equations, we used a similarity framework to convert them into a standardized set of dimensionless differential equations. The computational simulation was conducted using the bvp4c integrated package, which is readily accessible with MATLAB. By using the bvp4c package, we successfully conducted the computational simulation and acquired the anticipated outcomes. Before proceeding to the subsequent phase, we conducted a comprehensive analysis, built a mathematical model, solved the issue, and graphically displayed our findings.

2. Mathematical Formulation

This study is mostly about looking at the flow pattern that stays the same around a Casson nanofluid with a disk that spins, as shown in Figure 1. The Cylindrical coordinates (r, φ, z) which are used to compute the fluid momentum components (u, v, w). Due to the axisymmetric character of the flow along the z axis, It is usually agreed that there is no connection between the physical numbers because the flow is symmetric around the z-axis. The upper section of flow region filled with the Casson nanofluid. Stagnation points are positions on a line situated at a negative z-coordinate. The anticipated radial expansion and contraction of the disk are denoted by $u(r,0) = u_w = cr$ and $u_e(r,0) = dr$, The disk spins in the positive direction at a velocity indicated by $v(r,0) = v_w = r\Omega$, where Ω represents the rotational speed and it is non-negative. It is presumed that the angular velocity is higher than the rotational speed r. Moreover, it is anticipated that there exists a greater temperature gradient between the disk's surface (T_w) and the surrounding fluid (T_∞). The symbol C_∞ denotes the volumetric ratio of nanoparticles in the surrounding fluid. This research aims to examine the impacts of thermophoresis, Fourier heat flux, chemical reaction and Brownian motion caused by nanoparticles using the Buongiorno nanofluid model. The analysis of heat transfer properties of the nanofluid takes into account the variable thermal conductivity and melting heat.

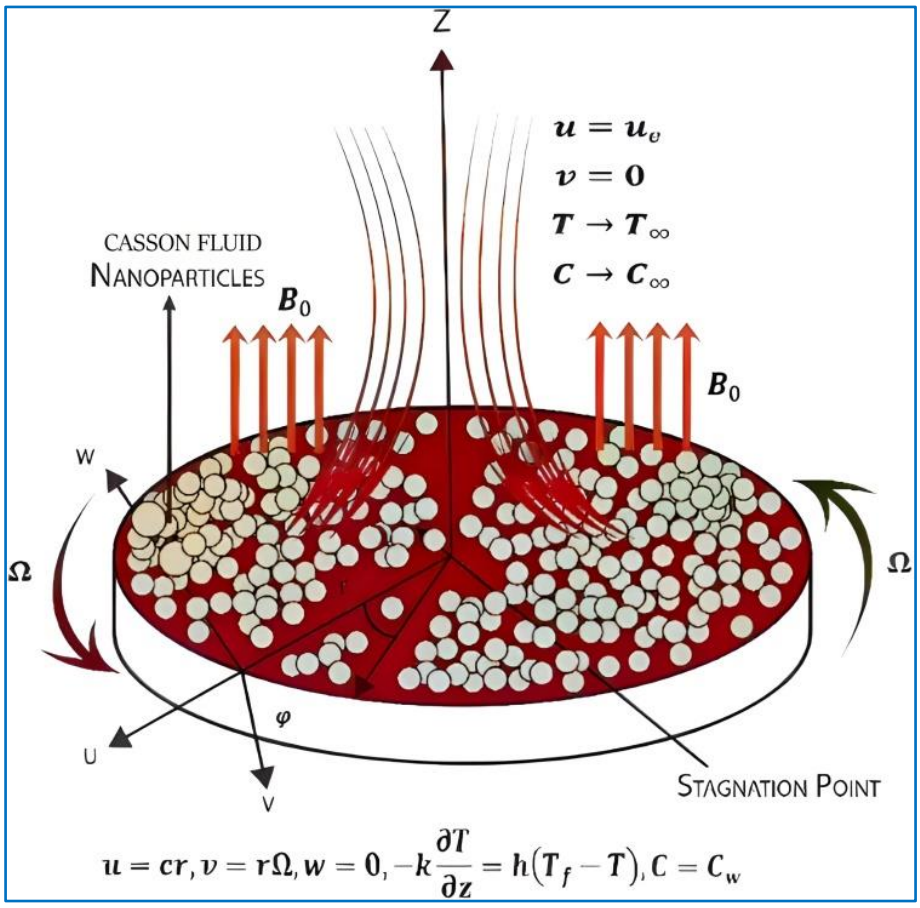

Figure 1. Flow structure illustration.

Considering certain assumptions and making approximations to the flow modeled by Rehman et al.(2018), Moatimid et al.(2022) and Ahmed et al.(2019).

$$\frac{\partial u}{\partial r} + \frac{u}{r} + \frac{\partial w}{\partial z} = 0 \tag{1}$$

$$\frac{\partial u}{\partial r} - \frac{v^2}{r} + w\frac{\partial u}{\partial z} - u_e\left(\frac{du_e}{dr}\right) - \vartheta_f\left(1 + \frac{1}{\beta}\right)\left(\left(\frac{\partial^2 u}{\partial r^2} + \frac{1}{r}\frac{\partial u}{\partial r} - \frac{u}{r^2}\right) + \frac{\partial^2 u}{\partial z^2}\right) = -\frac{\sigma}{\rho_f} B_o^2(u_e - u) \tag{2}$$

$$u\frac{\partial v}{\partial r}+\frac{uv}{r}+w\frac{\partial v}{\partial z}-\vartheta_f\left(1+\frac{1}{\beta}\right)\left(\frac{\partial^2 v}{\partial r^2}+\frac{1}{r}\frac{\partial v}{\partial r}-\frac{v}{r}+\frac{\partial^2 v}{\partial z^2}\right)=-\frac{\sigma}{\rho_f}B_o^2 v \quad (3)$$

$$u\frac{\partial T}{\partial r}+w\frac{\partial T}{\partial z}-\alpha_f\left(\frac{\partial^2 T}{\partial r^2}+\frac{\partial^2 T}{\partial z^2}+\frac{1}{r}\frac{\partial T}{\partial r}\right)=\tau\left(D_B\left(\frac{\partial T}{\partial r}\frac{\partial C}{\partial r}+\frac{\partial T}{\partial z}\frac{\partial C}{\partial Z}\right)+\frac{D_T}{T_\infty}\left(\left(\frac{\partial T}{\partial r}\right)^2+\left(\frac{\partial T}{\partial z}\right)^2\right)\right)-\lambda_1\left(u^2\frac{\partial^2 T}{\partial r^2}+w^2\frac{\partial^2 T}{\partial z^2}+2uw\frac{\partial^2 T}{\partial r\partial z}+\frac{\partial T}{\partial r}\left(u\frac{\partial u}{\partial r}+w\frac{\partial u}{\partial z}\right)+\frac{\partial T}{\partial z}\left(u\frac{\partial w}{\partial r}+w\frac{\partial w}{\partial z}\right)\right) \quad (4)$$

$$u\frac{\partial C}{\partial r}+w\frac{\partial C}{\partial z}=D_B\left(\frac{\partial^2 C}{\partial r^2}+\frac{1}{r}\left(\frac{\partial C}{\partial r}\right)+\frac{\partial^2 C}{\partial z^2}\right)+\left(\frac{D_T}{T_\infty}\right)\left(\frac{\partial^2 T}{\partial r^2}+\frac{1}{r}\left(\frac{\partial T}{\partial r}\right)+\frac{\partial^2 T}{\partial z^2}\right)-K_r(C-C_\infty) \quad (5)$$

The velocities in the radial, azimuthal, and axial directions are denoted by the variables u, v, and w, respectively. The equation takes into account many factors, such as the fluid temperature (T), the concentration of nanoparticles (C), the density(ρ_f), the thermal diffusivity(α_f), and the nanoparticles' capacity (τ).

The boundary conditions that include slip effects are presented [10] as follows:

$$\left.\begin{aligned} u=cr, v=r\Omega, w=0, -k\frac{\partial T}{\partial z}=h\left(T_f-T\right), C=C_w \; at \; \zeta=0 \\ u\to u_e, v\to 0, \; T\to T_\infty, C\to C_\infty \; at \; \zeta\to\infty \end{aligned}\right\} \quad (6)$$

Introduce the Similarity Transformations.

$$\zeta=\sqrt{\frac{\Omega}{\vartheta}}z, u=r\Omega F(\zeta), v=r\Omega G(\zeta), w=\sqrt{\Omega\vartheta}H(\zeta), \theta(\zeta)=\frac{T-T_\infty}{T_f-T_\infty}, \phi(\zeta)=\frac{C-C_\infty}{C_w-C_\infty} \quad (7)$$

(2), (3), (4), (5) and (6) take the form under the transformation (7).

$$H'+2F=0 \quad (8)$$

$$\left(1+\frac{1}{\beta}\right)F''-F^2-G^2-HF'+\varepsilon^2-M(\varepsilon-F)=0 \quad (9)$$

$$\left(1+\frac{1}{\beta}\right)G''-2GF-HG'-MG=0 \quad (10)$$

$$\Theta''-Pr\Theta'H+Pr\{Nb\Theta'\Phi'+Nt\Theta''-\gamma[\Theta''H^2+HH'\Theta']\}=0 \quad (11)$$

$$\Phi''+ScH\Phi'+\frac{Nt}{Nb}\Theta''-ScCr\Phi=0 \quad (12)$$

In addition to modified boundary conditions,

$$\left.\begin{aligned} F(0)=1, G(0)=\omega, H(0)=0, \; \Theta'(0)=-Bi\left(1-\Theta(0)\right), \; \Phi'(0)=1 \\ F(\zeta)\to\varepsilon, G(\zeta)\to 0, \Theta(\zeta)\to 0, \Phi(\zeta)\to 0; as \; \zeta\to\infty \end{aligned}\right\} \quad (13)$$

The dimensionless quantities involved are the magnetic parameter M and the velocity ratio parameter ε, Schmidt number (Sc), The Prandtl number (Pr), thermal relaxation parameter (γ), Brownian motion (Nb),

The chemical reaction parameter (Cr), Casson parameter is represented as β. The Thermal Biot number Bi, Thermophoresis (Nt) and the rotation parameter (ω).

$$M=\frac{\sigma^* B_o^2}{\Omega\rho_f}, \varepsilon=\frac{d}{\Omega}, Pr=\frac{\vartheta_f}{\alpha_f}, C_r=\frac{K_r}{C}, \; \omega=\frac{\Omega}{c}, \; Bi=\frac{h}{k}\sqrt{\frac{\vartheta_f}{2\Omega}}, \; Nb=\frac{\tau D_B(C_w-C_\infty)}{\vartheta_f}, \; Nt=\frac{\tau D_T\left(T_f-T_\infty\right)}{\vartheta_f}, \; Sc=\frac{\vartheta_f}{D}$$

The simplified form for drag force C_F , Nu_r Nusselt number, Sh_r Sherwood number as follows:

$$\left.\begin{aligned} C_F Re_r^{0.5}=\left(1+\frac{1}{\beta}\right)[F'^2(0)+G'^2(0)]^{0.5} \\ Nu_r Re_r^{-0.5}=-\Theta'(0) \\ Sh_r Re_r^{-0.5}=-\Phi'(0) \end{aligned}\right\} \quad (14)$$

$Re_r$is Local Reynolds number= $Re_r=\frac{ru_w}{\vartheta_f}$

3. Numerical Algorithm

The intricate system represented by Equations (9-13) is resolved via MATLAB's bvp4c technique. In order to use a numerical technique, it is necessary to transform Equations (9 to 13) into a set of first-order differential equations. Prior to advancing with the numerical answer, this transformation is required. The selected approach was considered the most suitable for illustrating the convergence criterion. The resultant system comprises differential equations of the first order.

$$\left.\begin{array}{c} F = y_1, F' = y_2, F'' = y_2' \\ G = y_3, G' = y_4, G'' = y_4' \\ H = y_5, H' = y_5' \\ \Theta = y_6, \Theta' = y_7, \Theta'' = y_7' \\ \Phi = y_8, \Phi' = y_9, \Phi'' = y_9' \end{array}\right\} \quad (15)$$

When the variables listed above are used, the first-order ODEs system is formed.

$$\left.\begin{array}{c} y_2' = \left(1+\frac{1}{\beta}\right)^{-1}[y_1^2 + y_3^2 + y_5 y_2 - \varepsilon^2 + M(\varepsilon + y_1)] \\ y_4' = \left(1+\frac{1}{\beta}\right)^{-1}[2y_3 y_1 + y_5 y_4 + M y_3] \\ y_7' = (1-\gamma Pr y_5^2)^{-1}[Pr\{\gamma y_5 y_5' y_7 - Nb y_7 y_9 - Nt y_7^2 + y_5 y_7\}] \\ y_9' = Sc y_5 y_9 - \frac{Nt}{Nb} y_7' + Sc C_r y_8 \end{array}\right\} \quad (16)$$

The corresponding boundary conditions converted as

$$\left.\begin{array}{c} y_1(0) = 1, y_3(0) = \omega, y_5(0) = 0, y_7(0) = -Bi\big(1 - y_6(0)\big), y_8(0) = 1 \ \ at\ \zeta = 0 \\ y_1(\zeta) \to \epsilon, y_3(\zeta) \to 0, y_6(\zeta) \to 0, y_8(\zeta) \to 0 \ \ at\ \zeta \to \infty \end{array}\right\} \quad (17)$$

4. Results and Discussion

We investigated the rheological properties of a Casson fluid induced by a revolving disk, with particular emphasis on the flow stagnation point. This flow scenario is characterized by the transfer of thermal energy via convection and the impact of magnetic fields. In addition, we investigated the impacts of heat flux and chemical processes. The particular attributes being examined were expressed as non-dimensional quantities. The relevant observations were recorded using visual illustrations and a structured table format. The aforementioned results were obtained using a computational methodology, especially the RK-4th order strategy, using the Bvp4c algorithm in MATLAB. The Table.1-Table.3 provide the variations in skin friction coefficient, Nusselt number, and Sherwood number, which were used to calculate numerical solutions.

Graphs 2(a-d) illustrate the variations in temperature distribution Θ(ζ), axial speed H(ζ), tangential speed G(ζ), and radial speed F(ζ) with increasing magnetic field strength M. Research has shown that the motion of nanofluids exhibits a reduction when subjected to more intense magnetic fields. The link between the electromagnetic force and the drag force is primarily characterized by the magnetic parameter M. Consequently, a higher value of M indicates that the drag force has a greater impact, resulting in a decrease in the radial speed F(ζ) and tangential speed G(ζ).

Table 1. Mathematical results for Skin friction $Re_r^{0.5} C_F$ through various values of Physical parameters

M	ω	ε	β	$C_F Re_r^{0.5}$
1	0.1	0.1	-	1.590051
1.2				1.665493
1.3				1.702177
1.4				1.738204
	0.2			1.624915
	0.3			1.681394
	0.4			1.757372

	0.5			1.850407
		0.2		1.706888
		0.3		1.741146
		0.4		1.757553
		0.5		1.755117
			0.2	1.782444
			0.3	1.747593
			0.4	1.723948
			0.5	1.706847

Table 2. The numerical results of the Nusselt number for a variety of physical parameter values.

Pr	γ	Nb	Nt	Bi	$Re_r^{-0.5}Nu_r$
1	0.1	0.2	0.3	0.2	0.577740
				0.3	0.61830
				0.4	0.623120
				0.5	0.674030
		0.3	0.4		0.507870
		0.4	0.5		0.53180
		0.5	0.6		0.54760
2					0.4537
3					0.3916
4					0.2776
	0.2				0.6213
	0.3				0.6421
	0.4				0.6835

Table 3. The numerical results for the Sherwood number based on a variety of physical parameter values.

Nt	Nb	Cr	Sc	$Sh_r Re_r^{-0.5}$
0.3	0.2	0.5	0.5	1.185090
			1.0	1.387322
			1.5	1.582412
			2.0	1.770033
		1.0		1.185090
		1.5		1.263887
		2.0		1.340345
		3.0		1.557089

On the other hand, as the magnetic field becomes stronger, there is an observed rise in the axial speed H(ζ). The relationship between the increasing magnetic parameters M and the distribution of temperature is seen in graph 2(d). This graph demonstrates a positive correlation between the magnetic strength and the thickness of the temperature and thermal layers. The resistance of the fluid rises as the magnetic parameter increases, resulting in increasing levels of friction and heat production, therefore raising the temperature of the fluid.

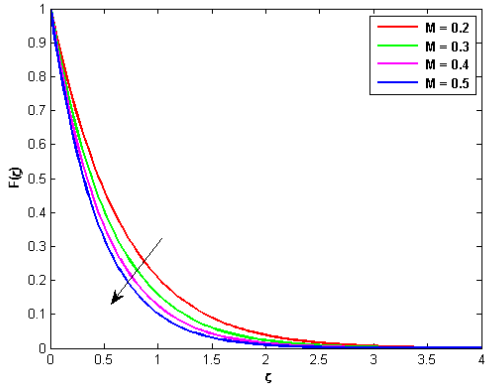

2(a)

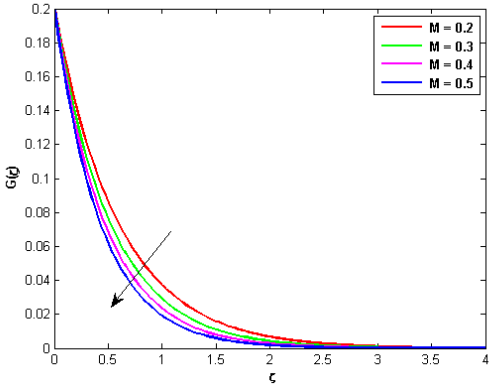

2 (b)

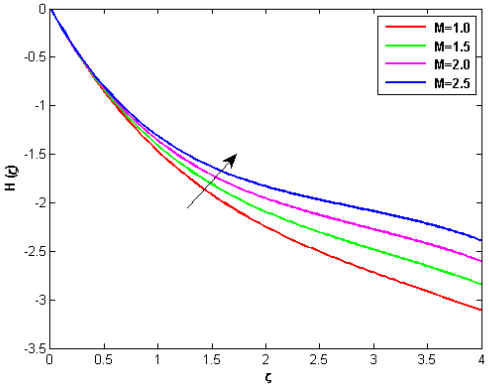

2(*c*)

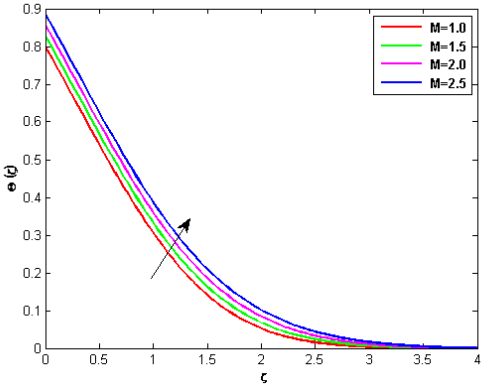

2(d)

Figure 2(a-d). Effects of M on $F(\zeta), G(\zeta), H(\zeta)$ and $\Theta(\zeta)$

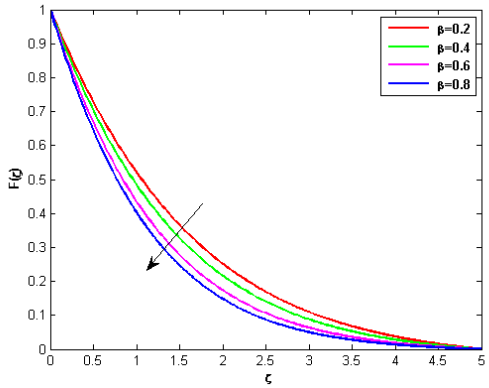

3(*a*)

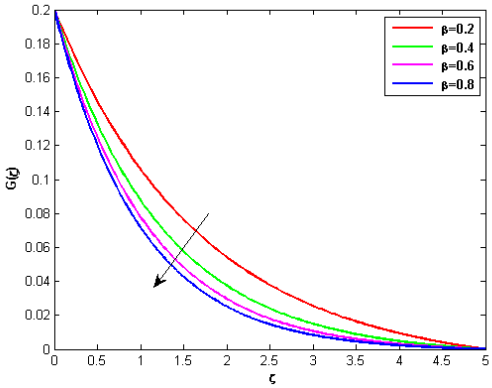

3(b)

Figure 3(a-b). The effect of β on $F(\zeta), G(\zeta)$

Graphs 3(a–d) depict the influence of the β parameter of the casson fluid on the radial, azimuthal, and axial velocities, as well as the temperature distribution. As the value of β grows, the speeds in the radial and azimuthal directions generally drop, while the profiles of axial speed and temperature tend to increase.

Thermal relaxation augmentation refers to an increase in the fluid's ability to adjust to changes in temperature, hence maintaining thermal equilibrium. Therefore, an escalation in the thermal relaxation parameter γ results in a decrease in both the temperature distribution and the thermal boundary layer, as seen in figure 4(a). More precisely, increasing the thermal relaxation value leads to a decrease in the amount of heat transferred from the surface of the disc to the fluid in its surroundings. Figure 4(b) demonstrates the influence of Bi on the Thermal profile. The Biot number determines the convective boundary condition at the rotating disk. As the Biot number grows, the temperature differential around the disk likewise increases, leading to a bigger thermal boundary layer.

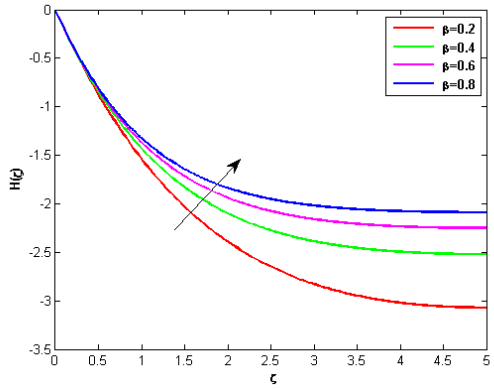

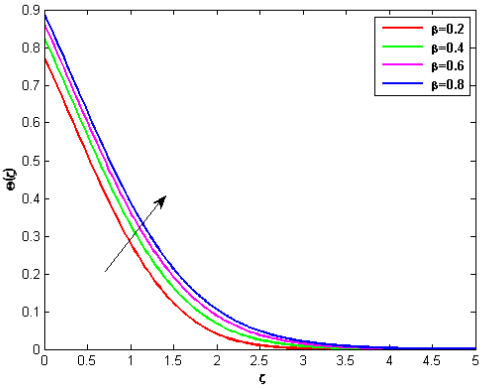

3(c) 3(d)

Figure 3(c-d). The effect of β on $H(\zeta)$ and $\Theta(\zeta)$

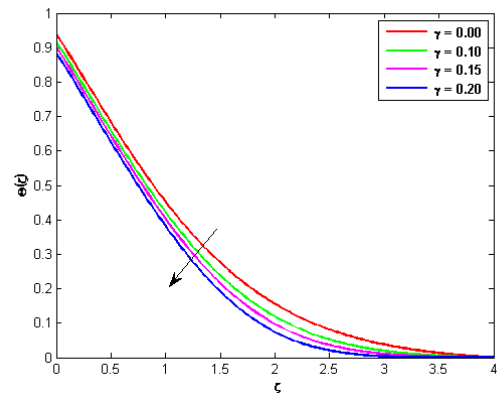

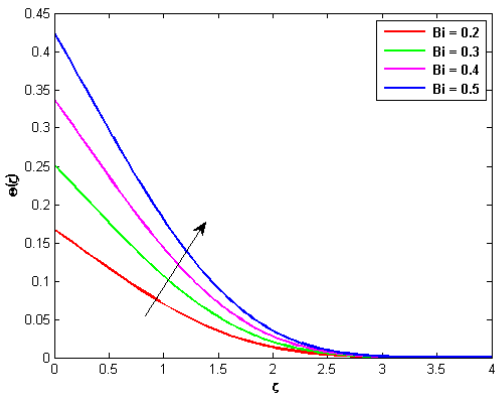

4(a) **4(b)**

Figure 4(a-b). Impact of γ, Bi on $\Theta(\zeta)$

Figure 4(c) demonstrates the impact of the Prandtl number (Pr) on the Θ(ζ). A greater Prandtl number leads to a reduction in the thickness of the thermal boundary layer. The Prandtl number, symbolized as Pr, is the ratio of momentum diffusivity to heat diffusivity. As the Prandtl number rises, the thermal diffusivity also increases, leading to a progressive decrease in temperature. Figures 5(a–b) exhibit identical patterns for the distributions of Nb in concentration Φ(ζ) and temperature Θ(ζ). There is a direct correlation between the thermophoresis factor and the magnitude of the dimensionless heat variable. From a scientific standpoint, it is clear that these characteristics enhance the heat capacity. This enhancement occurs due to the increased introduction of heat into the flow from the surface of the disc. When the value of the Brownian motion constant is low, the distribution pattern of substances becomes more discernible. As the value of Nb increases, the density of the material decreases, leading to a greater quantity and more intense interactions among the particles of the fluid.

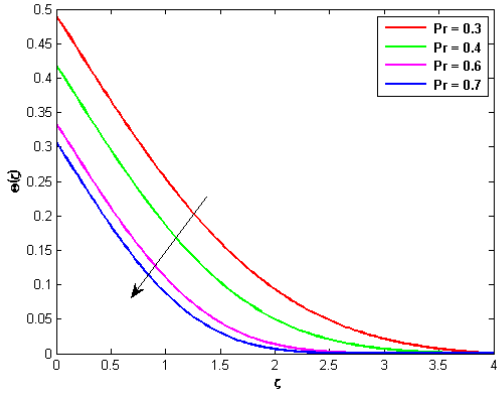

Figure 4(c). Impact of Pr on $\Theta(\zeta)$

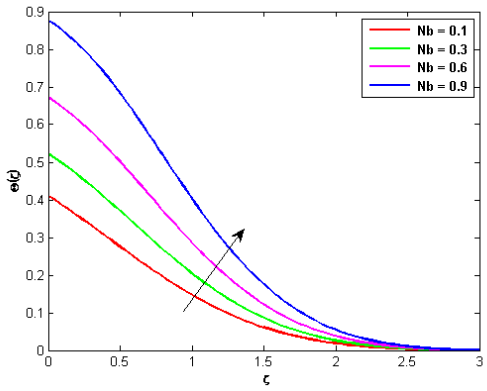

Figure 5(a). Influence of Nb on $\Theta(\zeta)$

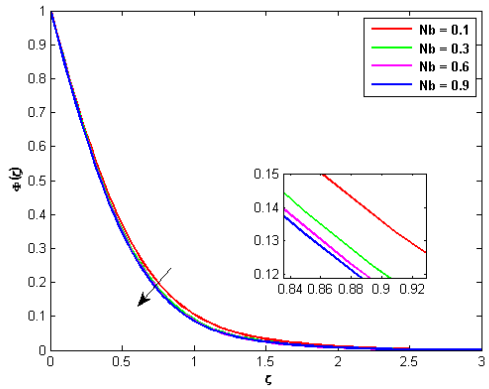

Figure 5(b). Influence of Nb on $\Phi(\zeta)$

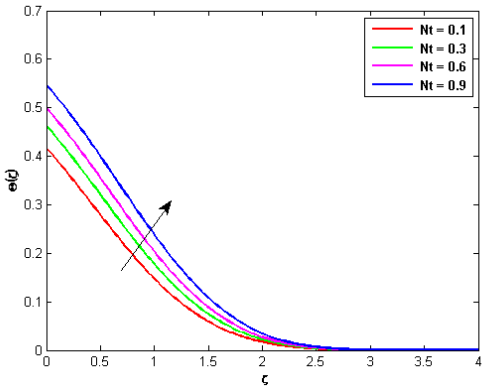

Figure 6(a). Influence of Nt on $\Theta(\zeta)$

Figure 6(a-b) depicts the impact of Nt on the thermal field Θ(ζ) and the concentration distribution Φ(ζ). It has been observed that the function Θ(ζ) enhances when the value of Nt grows. Increased levels of Nt are associated with more powerful thermophoretic forces and the subsequent movement of nanoparticles from warmer to cold surroundings. The temperature increases as a consequence. Figure 6(b) illustrates the relationship between the concentration and a thermophoresis factor, Nt. Increases exponentially with the value of Nt, as expected. Thermophoresis is the term used to describe the physical process by which nanoparticles are transferred from a higher temperature environment to a lower temperature environment. Consequently, the thickness of the boundary layer increases.

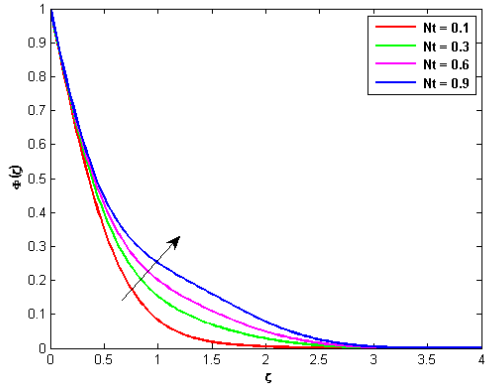

Figure 6(b). Influence of Nt on $\Phi(\zeta)$

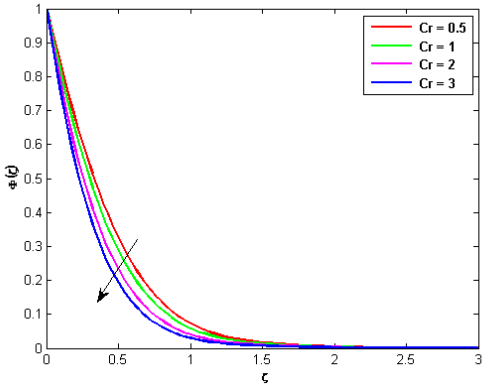

Figure 7(a). Influence of Cr on Φ(ζ)

Figure 7(a) demonstrates that a rise in the Schmidt number in an estimate is associated with a drop in concentration. The value Sc shows the ratio of viscosity to mass diffusivity. As a result, as the Sc (Schmidt number) increases, the concentration levels fall because the mass diffusivity is smaller than the viscosity. Figure 7(b) presents an examination of the interplay between species in a chemical reaction Cr and Φ(ζ). As the reaction rate rises, the concentration gradient reduces, which improves the accuracy of the parameters associated with the chemical reaction. The velocity distributions for the parameter associated with the velocity ratio (ε) are shown in Figure 8(a-c). By augmenting the stretching parameter, the boundary layer's thickness decreases, resulting in an elevation in radial velocity and a reduction in both axial and azimuthal velocities.

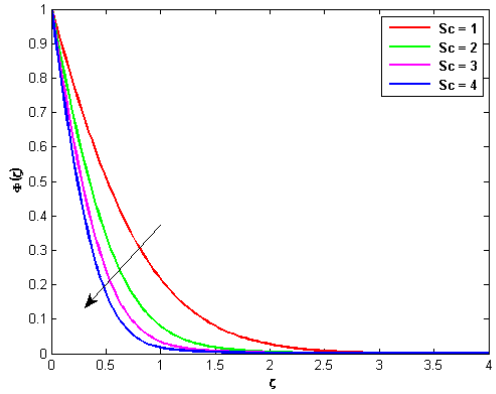

Figure 7(b). Influence of Sc on Φ(ζ)

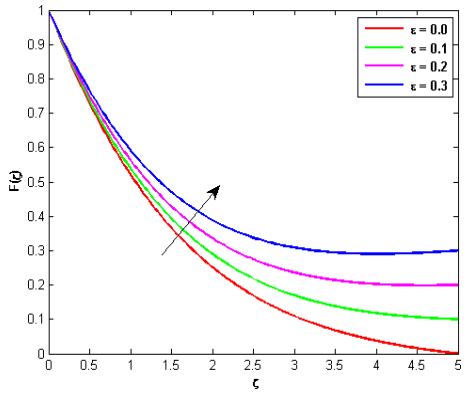

Figure 8(a). Influence of ε velocity ratio on $F(\zeta)$

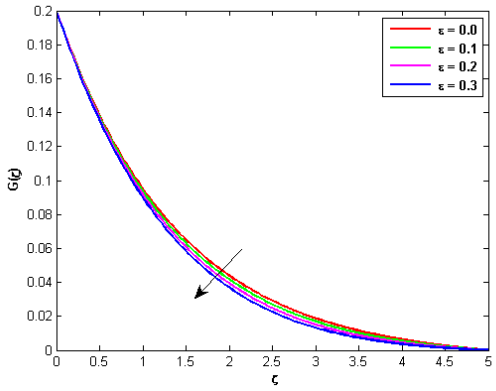

8(b)

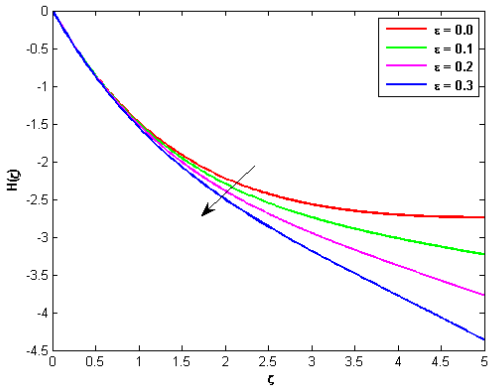

8(c)

Figure 8(b-c). Influence of ε velocity ratio on $G(\zeta)$, $H(\zeta)$

5. Conclusions

This study examines the MHD flow of a Casson nanofluid towards a disk that is expanding radially. This flow is characterized by convective boundary conditions and is influenced by the Christov heat flux. These governing partial differential equations are transformed into nonlinear ordinary differential equations by suitable similarity transformations. Afterwards, numerical solutions are computed using both the fourth-order Runge-Kutta method and the Shooting technique. The main discoveries from this research field are as follows.

i. Augmenting the Casson (β), magnetic (M) parameters thus thermal boundary layer thicker due to decreases radial and azimuthal velocity profiles. However, the tendency was reversed in terms of axial velocity.
ii. Increasing M, β, and Bi leads to increased thermal boundary layer thickness, whereas relaxation time γ and Pr have the inverse impact on the dispersion of thermal profile.
iii. Empirical evidence demonstrates that the concentration profile exhibits a decline as the amounts of Cr and Sc rise.

iv.While increasing the thermophoresis factor improves the distribution of concentrations, it diminishes as the Brownian motion factor Nb increases.

References

[1] Von KARMAN Th. (1921). Uber Laminare und Turbulente Reibung. Z. Angew. Math. Mech., 1, 233–252.
[2] Turkyilmazoglu, M., & Senel, P. (2013). Heat and mass transfer of the flow due to a rotating rough and porous disk. International Journal of Thermal Sciences, 63, 146–158. https://doi.org/10.1016/j.ijthermalsci.2012.07.013
[3] Rashidi, M., Kavyani, N., & Abelman, S. (2014). Investigation of entropy generation in MHD and slip flow over a rotating porous disk with variable properties. International Journal of Heat and Mass Transfer/International Journal of Heat and Mass Transfer, 70, 892–917. https://doi.org/10.1016/j.ijheatmasstransfer.2013.11.058
[4] Turkyilmazoglu, M. (2014). Nanofluid flow and heat transfer due to a rotating disk. Computers & Fluids, 94, 139–146. https://doi.org/10.1016/j.compfluid.2014.02.009
[5] Khan, A. S., Idrees, M., & Khan, N. U. S. (2023). Numerical examination of wall properties for the magnetohydrodynamics stagnation point flow of micro-rotating fluid subject to weak concentration. Physics of Fluids, 35(5). https://doi.org/10.1063/5.0142576
[6] Sulochana, N. C., Begum, N. S., & Kumar, N. T. P. (2023). MHD Mixed Convective Non-Newtonian Stagnation Point Flow Over an Inclined Stretching Sheet: Numerical Simulation. Journal of Advanced Research in Fluid Mechanics and Thermal Sciences, 102(1), 73–84. https://doi.org/10.37934/arfmts.102.1.7384
[7] Bakar, N. F. N. A., & Soid, N. S. K. (2023). MHD Stagnation-Point Flow and Heat Transfer in a Micropolar Fluid over an Exponentially Vertical Sheet. CFD Letters, 15(3), 81–96. https://doi.org/10.37934/cfdl.15.3.8196
[8] Dawar, A., Islam, S., Alshehri, A., Bonyah, E., & Shah, Z. (2022). Heat Transfer Analysis of the MHD Stagnation Point Flow of a Non-Newtonian Tangent Hyperbolic Hybrid Nanofluid past a Non-Isothermal Flat Plate with Thermal Radiation Effect. Journal of Nanomaterials, 2022, 1–12. https://doi.org/10.1155/2022/4903486
[9] Kotnurkar, A. S., & Mali, G. (2022). MHD Non-Aligned Stagnation-Point Flow of Nanofluid over a Stretching Surface with a Convective Boundary Condition. Engineering Science & Technology, 35–53. https://doi.org/10.37256/est.4120231965
[10] Rehman, K. U., Malik, M., Zahri, M., & Tahir, M. (2018). Numerical analysis of MHD Casson Navier's slip nanofluid flow yield by rigid rotating disk. Results in Physics, 8, 744–751. https://doi.org/10.1016/j.rinp.2018.01.017
[11] Li, S., Faizan, M., Ali, F., Ramasekhar, G., Muhammad, T., Khalifa, H. a. E. W., & Ahmad, Z. (2024). Modelling and analysis of heat transfer in MHD stagnation point flow of Maxwell nanofluid over a porous rotating disk. Alexandria Engineering Journal /Alexandria Engineering Journal, 91, 237–248. https://doi.org/10.1016/j.aej.2024.02.002
[12] Hannah, D. M. (1947). Forced flow against a rotating disc. https://reports.aerade.cranfield.ac.uk/handle/1826.2/3325
[13] Agrawal, H. L. (1957). A new exact solution of the equations of viscous motion with axial symmetry. Quarterly Journal of Mechanics and Applied Mathematics, 10(1), 42–44. https://doi.org/10.1093/qjmam/10.1.42
[14] Rehman, A. U., Riaz, M. B., Atangana, A., Jarad, F., & Awrejcewicz, J. (2022). Thermal and concentration diffusion impacts on MHD Maxwell fluid: A generalized Fourier's and Fick's perspective. Case Studies in Thermal Engineering, 35, 102103. https://doi.org/10.1016/j.csite.2022.102103
[15] Hayat, T., Sajjad, R., Alsaedi, A., Muhammad, T., & Ellahi, R. (2017). On squeezed flow of couple stress nanofluid between two parallel plates. Results in Physics, 7, 553–561. https://doi.org/10.1016/j.rinp.2016.12.038
[16] Choi, S. (1995). Enhancing thermal conductivity of fluids with nanoparticles, developments and applications of non-newtonian flows. https://cir.nii.ac.jp/crid/1571980074227838464

[17] Nadeem, S., Haq, R. U., & Lee, C. (2012). MHD flow of a Casson fluid over an exponentially shrinking sheet. Scientia Iranica, 19(6), 1550–1553. https://doi.org/10.1016/j.scient.2012.10.021
[18] Mukhopadhyay, S. (2013). Casson fluid flow and heat transfer over a nonlinearly stretching surface. Chinese Physics B/Chinese Physics B, 22(7), 074701. https://doi.org/10.1088/1674-1056/22/7/074701
[19] Mahanta, G., & Shaw, S. (2015). 3D Casson fluid flow past a porous linearly stretching sheet with convective boundary condition. Alexandria Engineering Journal /Alexandria Engineering Journal, 54(3), 653–659. https://doi.org/10.1016/j.aej.2015.04.014
[20] Waqas, H., Naseem, R., Muhammad, T., & Farooq, U. (2021). Bioconvection flow of Casson nanofluid by rotating disk with motile microorganisms. Journal of Materials Research and Technology/Journal of Materials Research and Technology, 13, 2392–2407. https://doi.org/10.1016/j.jmrt.2021.05.092
[21] Bixapathi, S., & Babu, A. B. (2024). Magnetic field influence on Casson fluid flow in rotating convection. Physics of Fluids, 36(5). https://doi.org/10.1063/5.0201977
[22] Noreen, S., Farooq, U., Waqas, H., Fatima, N., Alqurashi, M. S., Imran, M., Akgül, A., & Bariq, A. (2023). Comparative study of ternary hybrid nanofluids with role of thermal radiation and Cattaneo-Christov heat flux between double rotating disks. Scientific Reports, 13(1). https://doi.org/10.1038/s41598-023-34783-8
[23] Samantaray, S. S., Azam, M., Abbas, N., Misra, A., & Nayak, M. K. (2023). Impact of Cattaneo–Christov double diffusion theory and Arrhenius pre-exponential factor law on flow of radiative Reiner–Rivlin nanofluid over rotating disk. International Journal of Modern Physics B/International Journal of Modern Physics B. https://doi.org/10.1142/s0217979224501029
[24] Zeb, H., Bhatti, S., Khan, U., Wahab, H. A., Munir, T., & Malik, M. Y. (2023). Cattaneo–Christov heat flux modeling in nanofliuid TiO2–titanium oxide and aggregation nanoparticle flow between two rotating disks. Waves in Random and Complex Media, 1–21. https://doi.org/10.1080/17455030.2023.2193850
[25] Moatimid, G. M., Mohamed, M. a. A., & Elagamy, K. (2022). Heat and mass flux through a Reiner–Rivlin nanofluid flow past a spinning stretching disc: Cattaneo–Christov model. Scientific Reports, 12(1). https://doi.org/10.1038/s41598-022-18609-7
[26] Habu, P. N., Al'Aidrus, S. N., Noor, N. F. M., & Siri, Z. (2022). Mass Transfer of a Thermally Radiative MHD Cattaneo-Christov Nanofluid between Two Stretchable Spinning Disks. Sains Malaysiana, 51(7), 2223–2235. https://doi.org/10.17576/jsm-2022-5107-23
[27] Ali, U., Irfan, M., Rehman, K. U., Alqahtani, A. S., Malik, M. Y., & Shatanawi, W. (2022). On the Cattaneo–Christov heat flux theory for mixed convection flow due to the rotating disk with slip effects. Waves in Random and Complex Media, 1–15. https://doi.org/10.1080/17455030.2022.2056659
[28] Ahmed, J., Khan, M., Ahmad, L., Alzahrani, A. K., & Alghamdi, M. (2019). Thermally radiative flow of Maxwell nanofluid over a permeable rotating disk. Physica Scripta, 94(12), 125016. https://doi.org/10.1088/1402-4896/ab3b9a